Supplementary Information

A flexibility-pneumatic triboelectric nanogenerator for stable output of irregular wave energy

Jianlong Wang[1,2,4], Zheng Yang[1,2,4], Zhenjie Wang[1,4], Xinxian Wang[1,2], Yanrui Zhao[1,2], Jinbiao Ma[1,2], Hengyu Li[1,2], Yang Yu[1,2,*], Zhong Lin Wang[1,3,*], Tinghai Cheng[1,2,3,*]

[1] *Beijing Institute of Nanoenergy and Nanosystems, Chinese Academy of Sciences, Beijing 101400, China*
[2] *School of Nanoscience and Engineering, University of Chinese Academy of Sciences, Beijing 100049, China*
[3] *Guangzhou Institute of Blue Energy, Knowledge City, Huangpu District, Guangzhou 510555, China*
[4] *These authors contributed equally: Jianlong Wang, Zheng Yang, Zhenjie Wang.*
*Corresponding authors' e-mail addresses: yuyang@binn.cas.cn, zhong.wang@mse.gatech.edu, chengtinghai@binn.cas.cn.

This file includes:

Supplementary Figures:

Supplementary Table:

Supplementary Table 1 Comparison of the transferred charge of TEE-TENG with other reported works.

Supplementary Notes:

Supplementary Note 1 Analysis of the Forces Exerted by Internal Gas Particles on the Walls.

Supplementary Note 2 Analysis of the Interaction Forces Between the Driving Component and the Follower.

Supplementary Videos:

Supplementary Video 1 Ten 30 W LED lights can be illuminated.

Supplementary Video 2 Wireless temperature sensor can be powered by the FP-TENG.

Supplementary Video 3 The water quality sensor can be powered by the FP-TENG.

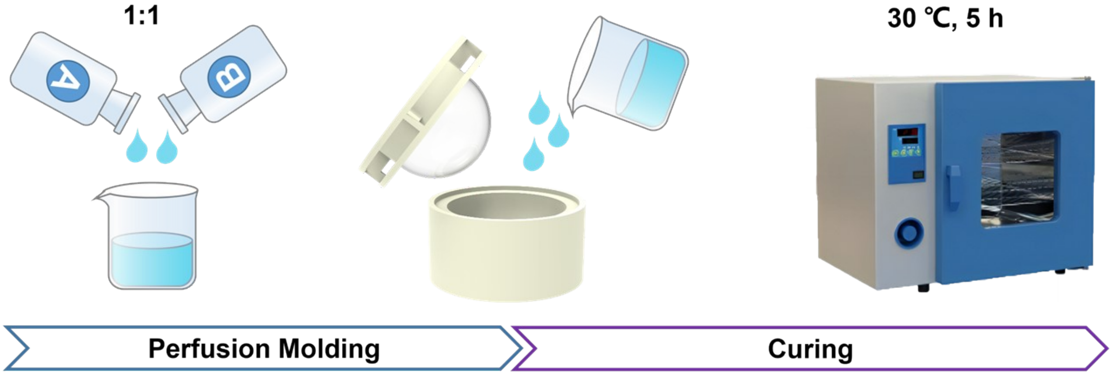

Supplementary Fig. 1 Fabrication process of the silicone spherical shell.

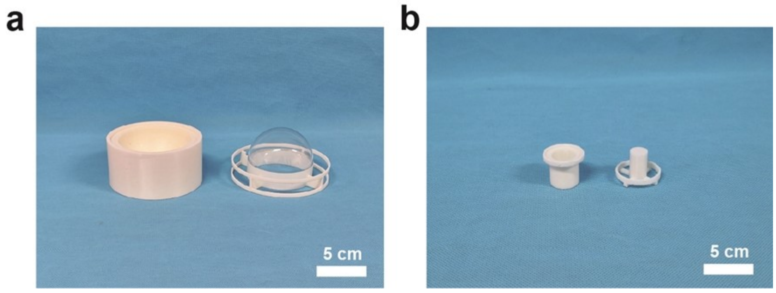

Supplementary Fig. 2 Molds used for silicone infusion.
(a) Pouring mold for flexible ball.
(b) Pouring mold for a cylinder.

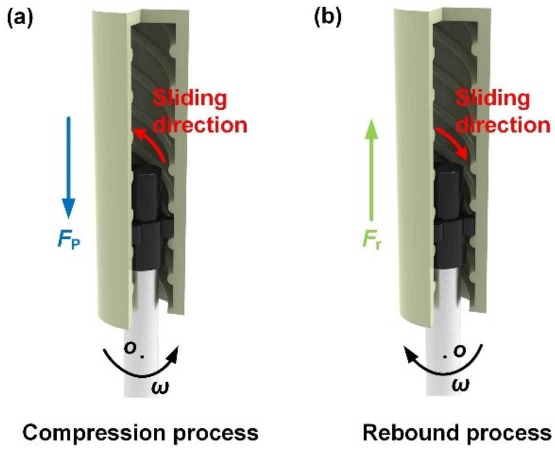

Supplementary Fig. 3 Schematic diagram of the working principle of the transmission mechanism.

(a) Compression process.

(b) Rebound process.

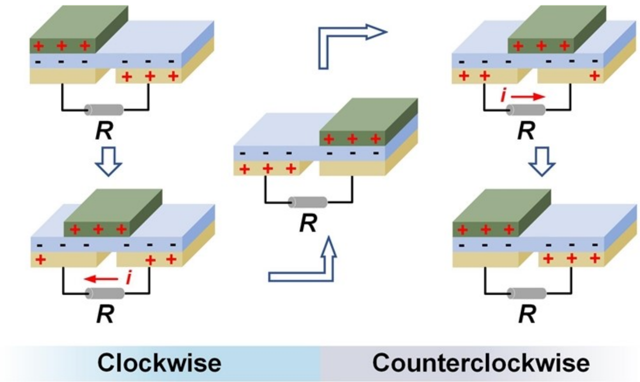

Supplementary Fig. 4 Working principle of the power generation unit.

Supplementary Fig. 5 Four-helix structures with different pitches.

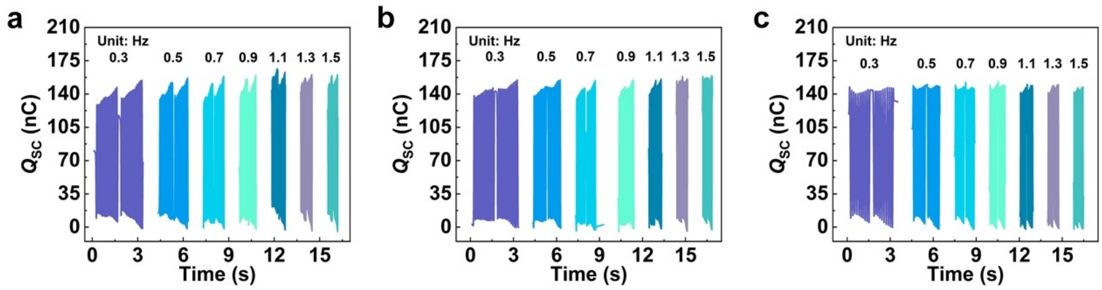

Supplementary Fig. 6 Output charge at different excitation frequencies for varying pitches.
(a) 20 mm.
(b) 25 mm.
(c) 30 mm.

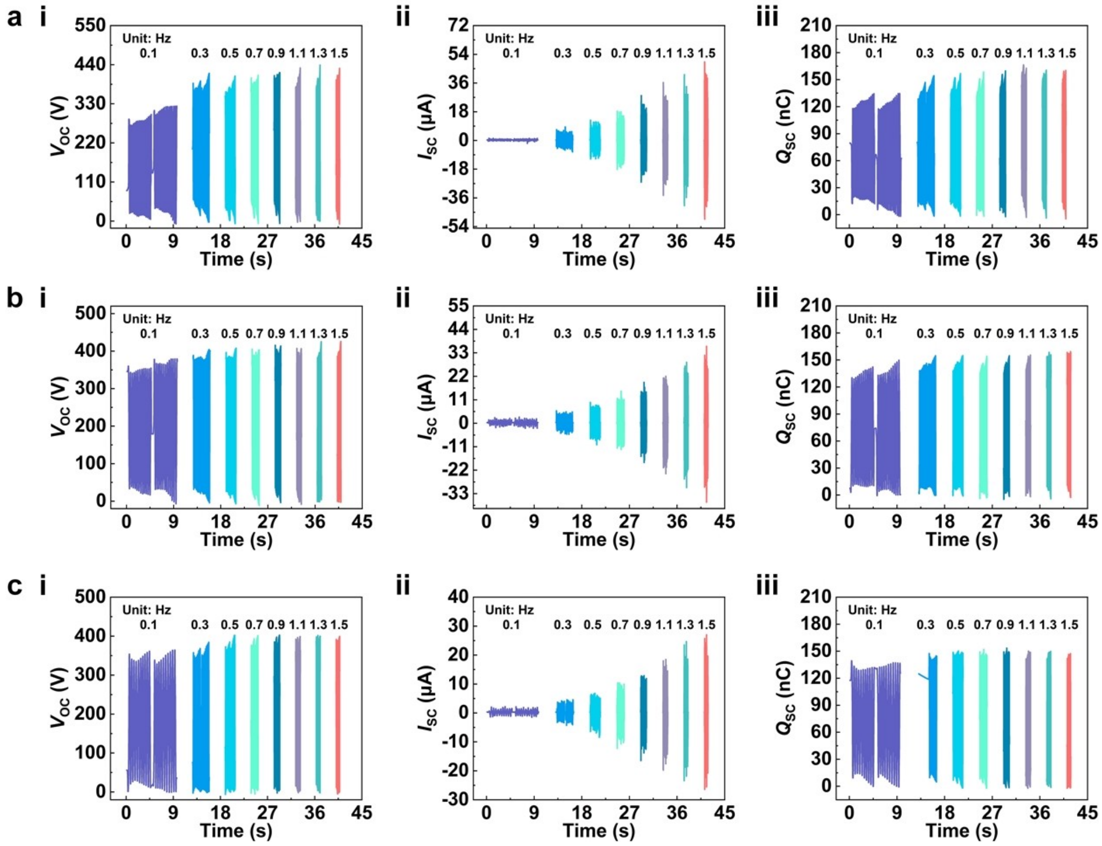

Supplementary Fig. 7 Specific output waveform under different external excitations at different pitches.

(a) 20 mm.

(b) 25 mm.

(c) 30 mm.

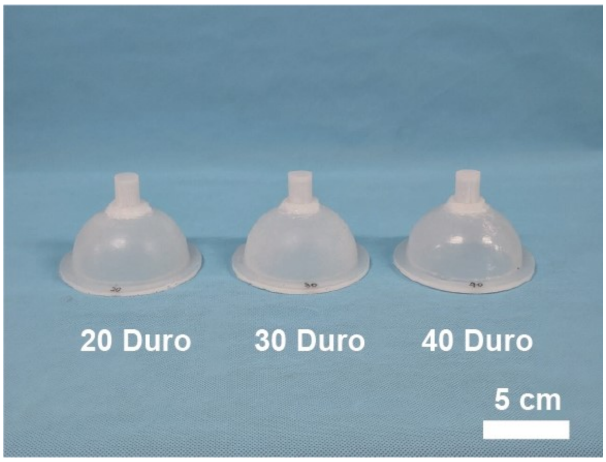

Supplementary Fig. 8 Flexible shells with different duros.

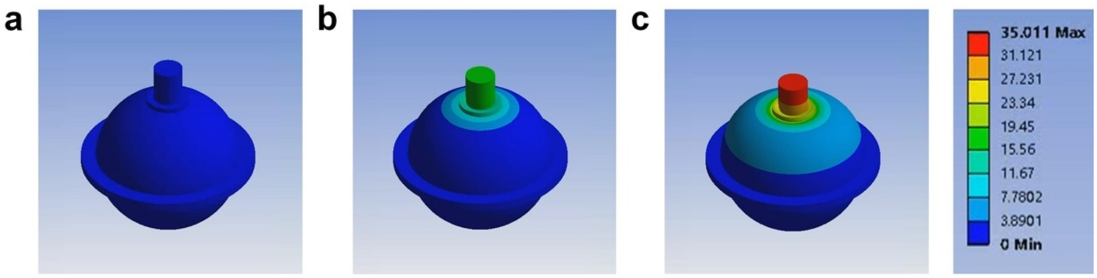

Supplementary Fig. 9 The force simulation analysis of flexible shell in the compression process.

(a) Initial state.

(b) Intermediate state.

(c) Fully compressed state.

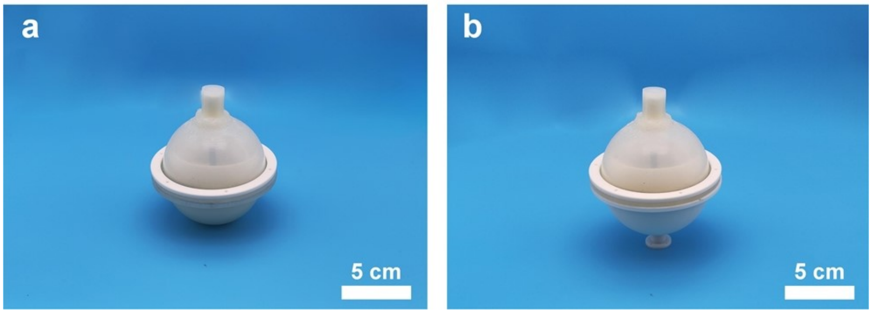

Supplementary Fig. 10 Pressure change curve for the 40 duro shell combined with soft and hard shells.

(a) Flexible shell with flexible shell (FF).

(b) Flexible shell with rigid shell (FR).

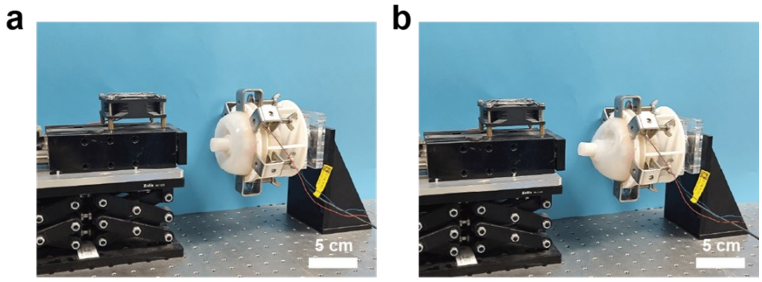

Supplementary Fig. 11 Condition changes of the spherical shell without gas under external stretching.
(a) Initial state.
(b) Tensile state.

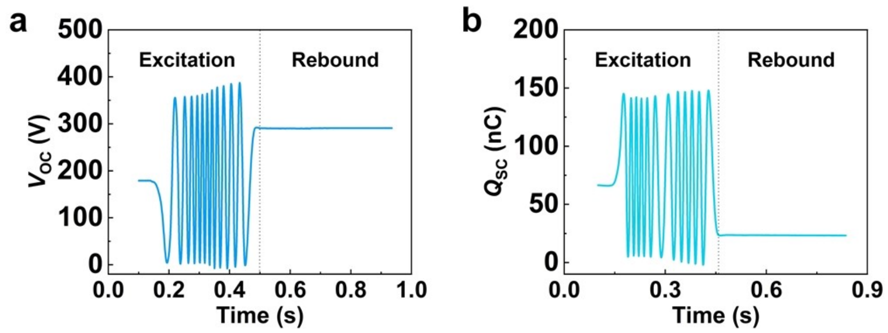

Supplementary Fig. 12 Voltage (a) and charge (b) output after stretching of the flexible body without gas.

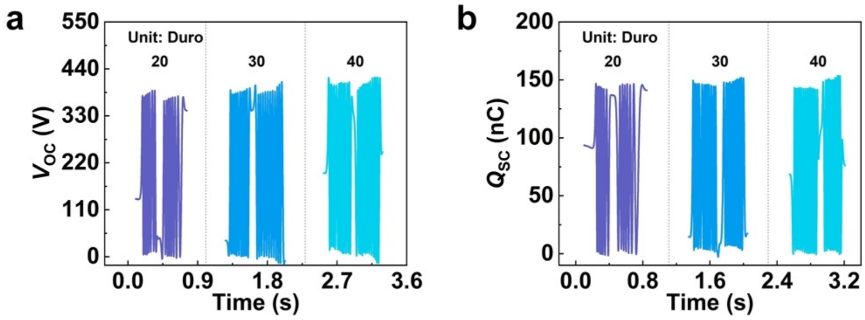

Supplementary Fig. 13 Voltage (a) and charge (b) generated by compression and rebound of the flexible body with different duros.

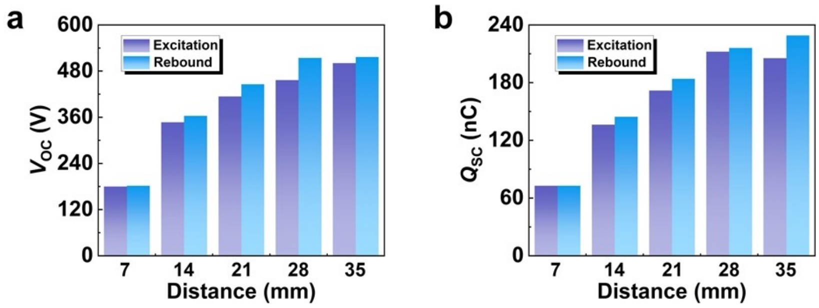

Supplementary Fig. 14 Voltage (a) and charge (b) of the FP-TENG during compression and rebound under varying compression distances.

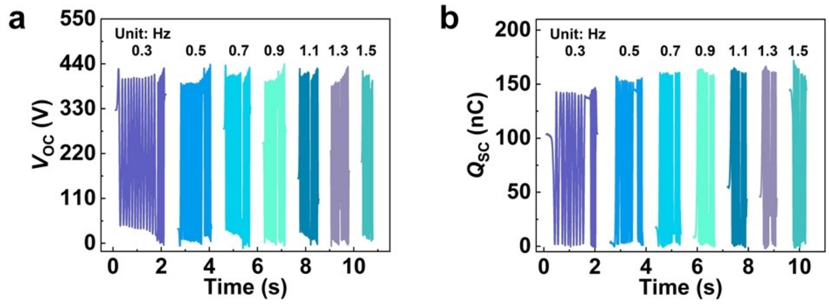

Supplementary Fig. 15 Voltage (a) and charge (b) of the FP-TENG during compression and rebound at different excitation frequencies.

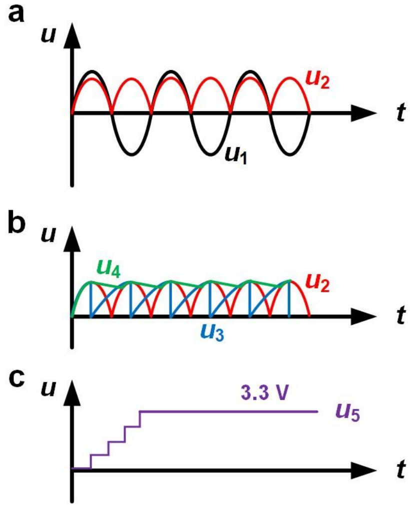

Supplementary Fig. 16 The variation diagram of the voltage waveform.
(a) The rectification process.
(b) The DC/DC conversion process.
(c) The voltage regulation process.

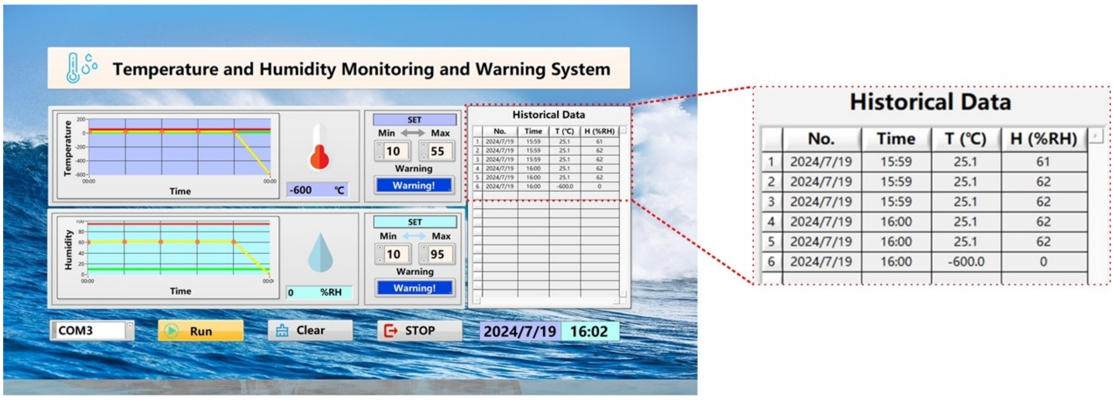

Supplementary Fig. 17 Display interface of sensor transmission data.

Supplementary Table 1 Comparison of the power density of FP-TENG with the reported works over the past year.

Series	Power density (W/m^3)	References
1	4.45	*Advanced Energy Materials*, 2024, 2402781[1]
2	13	*Cell Reports Physical Science*, 2024, **5**, 101933[2]
3	14.1	*Advanced Energy Materials*, 2023, **13**, 2203219[3]
4	14.56	*Chemical Engineering Journal*, 2024, **496**, 153738[4]
5	16.99	*Energy & Environmental Science*, 2023, **16**, 473–483[5]
6	20.6	*Joule*, 2024, **8**, 1855–1868[6]
7	28.9	*Advanced Functional Materials*, 2024, 2406775[7]
8	32.55	*Advanced Energy Materials*, 2024, **14**, 2400313[8]
9	34.26	This work

Supplementary Note 1 Analysis of the Forces Exerted by Internal Gas Particles on the Walls.

The stress acting on fluid particles can be divided into normal stress $\mathrm{d}F_{\mathrm{n}}$ (the stress that generates a force perpendicular to the surface of the fluid particles) and shear stress $\mathrm{d}F_{\tau}$ (the stress that generates a force parallel to the surface of the particles). Normal stress tends to compress the fluid particles without altering their shape.

When the gas is enclosed in a container, the gas molecules move freely and bounce off the container walls. Upon colliding with the walls, the molecules undergo elastic collisions, meaning that the magnitude of their energy and momentum remains constant. However, their direction of motion changes, indicating that the wall must exert a force on the gas molecules. Consequently, during the collision, the gas molecules exert an equal and opposite force on the wall. The force exerted on a small surface element $\mathrm{d}A$ due to the pressure p acting on one side of the element is given by:

$$\mathrm{d}F = -p\mathrm{d}A \tag{S1}$$

The force generated by pressure acts on the particles of a compressible fluid. This type of strain is referred to as volumetric strain, which is measured by the change in volume fraction $\mathrm{d}v/v$, where v represents the volume of the fluid particles. The pressure change $\mathrm{d}p$ required to induce this volumetric change is linearly related to the volumetric strain through the bulk modulus K. In other words,

$$\mathrm{d}p = -K\frac{\mathrm{d}v}{v} \tag{S2}$$

where the negative sign indicates that an increase in pressure results in a decrease in volume. We can express this in terms of the fractional change in density, where the fluid's density ρ is defined as its mass divided by its volume. Given that the mass of the particles m is constant,

$$v = \frac{m}{\rho} \tag{S3}$$

$$\frac{\mathrm{d}v}{v} = \frac{\mathrm{d}(m/\rho)}{(m/\rho)} = \rho\mathrm{d}\left(\frac{1}{\rho}\right) = -\frac{\mathrm{d}\rho}{\rho} \tag{S4}$$

According to Equations (2) and (4),

$$dp = K\frac{\mathrm{d}\rho}{\rho} \tag{S5}$$

$$p = \int \mathrm{d}p = K\int\frac{\mathrm{d}\rho}{\rho} = K\ln\rho + \mathrm{C} \tag{S6}$$

The force acting at that point is given by

$$\mathrm{d}F = -p\mathrm{d}A = -(K\ln\rho + \mathrm{C})\mathrm{d}A \tag{S7}$$

Supplementary Note 2 Analysis of the Interaction Forces Between the Driving Component and the Follower.

The driving force F_p generated by the drive component is decomposed into two components: a tangential force and a normal force.

$$\vec{F}_p = \vec{F}_{px} + \vec{F}_{py} \tag{S8}$$

The tangential component of the driven force F_{px}, is responsible for driving the rotational motion of the follower. The resistance generated during operation can be categorized into two primary components: the first is the frictional force f_1 produced by the driven component,

$$f_1 = \mu F_{py} \tag{S9}$$

where μ is the coefficient of friction. The second component is the frictional force f_2 generated by the power generation unit during its operation.

$$f_2 = \mu F_N \tag{S10}$$

The normal force F_C is composed of the contact force between dielectric materials and the electrostatic adhesion force F_E:

$$F_N = F_C + F_E \tag{S11}$$

Assuming that the positive dielectric material and the negative dielectric material in the power generation unit carry equal but opposite charges σ, the electric field generated by positive dielectric material (or negative dielectric material) can be expressed as:

$$E = \frac{\sigma}{2\varepsilon_0} \tag{S12}$$

The adhesive force F_N exerted by positive dielectric material on negative dielectric material can be represented as:

$$F_N = \sigma E A = \frac{A_E \sigma^2}{2\varepsilon_0} \tag{S13}$$

Based on Equations (9), (10), (11), and (13), the frictional force generated during operation can be derived as follows:

$$f = f_1 + f_2 = \mu(F_{py} + F_N) = \mu(F_{py} + F_C + \frac{A_E \sigma^2}{2\varepsilon_0}) \tag{S14}$$

References

1 Zhou, W. *et al.* Four-Helix Triboelectric Nanogenerator Based on Wave Amplitude Amplifier. *Advanced Energy Materials* **15**, 2402781 (2024).

2 Hong, H. *et al.* Omnidirectional water wave energy harvesting by a spherical triboelectric nanogenerator with sliced-pizza-shaped electrodes. *Cell Reports Physical Science* **5**, 101933 (2024).

3 Han, J., Liu, Y., Feng, Y., Jiang, T. & Wang, Z. L. Achieving a Large Driving Force on Triboelectric Nanogenerator by Wave-Driven Linkage Mechanism for Harvesting Blue Energy toward Marine Environment Monitoring. *Advanced Energy Materials* **13**, 2203219 (2023).

4 Cao, C. *et al.* Electro-mechano transduction of stacked triboelectric nanogenerator considering wave force: Modeling, validation and applications. *Chemical Engineering Journal* **496**, 153738 (2024).

5 Qiu, H., Wang, H., Xu, L., Zheng, M. & Wang, Z. L. Brownian motor inspired monodirectional continuous spinning triboelectric nanogenerators for extracting energy from irregular gentle water waves. *Energy & Environmental Science* **16**, 473-483 (2023).

6 Yu, Y. *et al.* Substantially boosting performance of triboelectric nanogenerators via a triboelectrification enhancement effect. *Joule* **8**, 1855-1868 (2024).

7 Chen, C. *et al.* One Meter Triboelectric Nanogenerator for Efficient Harvesting of Meter-Scale Wave Energy. *Advanced Functional Materials* **34**, 2406775 (2024).

8 Li, T. *et al.* Bidirectional Rotating Turbine Hybrid Triboelectric-Electromagnetic Wave Energy Harvester for Marine Environment Monitoring. *Advanced Energy Materials* **14**, 2400313 (2024).